Selective interleukin-1 receptor–associated kinase 4 inhibitors for the treatment of autoimmune disorders and lymphoid malignancy

Priscilla N. Kelly,[1] Donna L. Romero,[2] Yibin Yang,[1] Arthur L. Shaffer III,[1] Divya Chaudhary,[2] Shaughnessy Robinson,[3] Wenyan Miao,[2] Lixin Rui,[1] William F. Westlin,[2] Rosana Kapeller,[2] and Louis M. Staudt[1]

[1]Lymphoid Malignancies Branch, Center for Cancer Research, National Cancer Institute, National Institutes of Health, Bethesda, MD 20892
[2]Nimbus Therapeutics, Cambridge, MA 02141
[3]Schrödinger, New York, NY 10036

Pathological activation of the Toll-like receptor signaling adaptor protein MYD88 underlies many autoimmune and inflammatory disease states. In the activated B cell–like (ABC) subtype of diffuse large B cell lymphoma (DLBCL), the oncogenic *MYD88* L265P mutation occurs in 29% of cases, making it the most prevalent activating mutation in this malignancy. IRAK4 kinase accounts for almost all of the biological functions of MYD88, highlighting IRAK4 as a therapeutic target for diseases driven by aberrant MYD88 signaling. Using innovative structure-based drug design methodologies, we report the development of highly selective and bioavailable small molecule IRAK4 inhibitors, ND-2158 and ND-2110. These small molecules suppressed LPS-induced TNF production, alleviated collagen-induced arthritis, and blocked gout formation in mouse models. IRAK4 inhibition promoted killing of ABC DLBCL lines harboring *MYD88* L265P, by down-modulating survival signals, including NF-κB and autocrine IL-6/IL-10 engagement of the JAK–STAT3 pathway. In ABC DLBCL xenograft models, IRAK4 inhibition suppressed tumor growth as a single agent, and in combination with the Bruton's tyrosine kinase (BTK) inhibitor ibrutinib or the Bcl-2 inhibitor ABT-199. Our findings support pharmacological inhibition of IRAK4 as a therapeutic strategy in autoimmune disorders, in a genetically defined population of ABC DLBCL, and possibly other malignancies dependent on aberrant MYD88 signaling.

The Journal of Experimental Medicine

Autoimmune disorders and B cell malignancies arise from pathological expansion of B lymphocytes. In autoimmune diseases, B cells react to self-antigens using both the B cell receptor (BCR) and TLRs (Leadbetter et al., 2002; Lau et al., 2005; Ehlers et al., 2006; Marshak-Rothstein, 2006; Green and Marshak-Rothstein, 2011). Activation of TLRs (except TLR3) recruits the signaling adaptor protein MYD88, which engages the interleukin-1 receptor–associated kinases IRAK4 and IRAK1, thereby activating the NF-κB and type-1 IFN pathways to promote survival and expansion of autoantibody-producing B cells (Leadbetter et al., 2002; Lau et al., 2005).

In the activated B cell–like (ABC) subtype of diffuse large B cell lymphoma (DLBCL), recurrent mutations targeting the MYD88 TIR domain occur in 39% of cases, with one dominant mutation, L265P, occurring in 29% of cases (Ngo et al., 2011). *MYD88* L265P is absent or rare in most other subtypes of lymphoma, including the germinal center B cell–like (GCB) DLBCL subtype (Ngo et al., 2011). MYD88 L265P is unique among MYD88 mutant isoforms in its ability to coordinate a stable signaling complex involving IRAK4 and IRAK1, in which IRAK4 phosphorylates IRAK1, causing constitutive NF-κB activation, type I IFN signaling, and autocrine IL-6/IL-10 engagement of the JAK–STAT3 pathway (Ngo et al., 2011). The ability of mutant MYD88 to sustain the survival of ABC DLBCL cell lines requires the kinase activity of IRAK4, whereas IRAK1 kinase activity is dispensable; however, IRAK1 protein appears to perform a necessary scaffolding function (Ngo et al., 2011). Together, these data support the development of IRAK4-selective kinase inhibitors for the treatment of ABC DLBCL tumors expressing oncogenic MYD88 mutant isoforms.

The design of inhibitors of BCR signaling is a major focus of therapeutic development for the treatment of ABC DLBCL, given the dependence of ABC DLBCL on BCR signaling and the fact that gain-of-function mutations targeting the BCR subunits CD79A and CD79B occur frequently in

Correspondence to Louis M. Staudt: lstaudt@mail.nih.gov

L. Rui's present address is Dept. of Medicine, University of Wisconsin-Madison, Madison, WI 53792.

Abbreviations used: ABC, activated B cell like; BCR, B cell receptor; BTK, Bruton's tyrosine kinase; CI, combination index; Dex, dexamethasone; DLBCL, diffuse large B cell lymphoma; Fa, fraction affected; GCB, germinal center B cell like; MSU, monosodium urate; Syk, spleen tyrosine kinase; WBC, white blood cell.

The Rockefeller University Press $30.00
J. Exp. Med. 2015 Vol. 212 No. 13 2189–2201
www.jem.org/cgi/doi/10.1084/jem.20151074

this lymphoma subtype (Davis et al., 2010). Although the role of MYD88 in maintaining viability of ABC DLBCL lines is equally important (Ngo et al., 2011), the utility of small molecule therapeutics targeting MYD88 signaling remains largely undetermined. Given that IRAK4 mediates most, if not all, of the biological effects of MYD88, inhibition of IRAK4 is an attractive therapeutic approach to block pathological MYD88 signaling (Kawai et al., 1999; Suzuki et al., 2002; Kim et al., 2007). However, despite great interest in IRAK4 as a therapeutic target, the development of selective inhibitors has been confounded by the challenging structure of the IRAK4 catalytic domain. In addition, the generation of small molecules with the necessary properties suitable for in vivo testing has proven difficult (Wang et al., 2009; Chaudhary et al., 2015), leaving the potential of IRAK4 targeting in human malignancies relatively unexplored. In this study, we describe the discovery, properties, and initial in vivo pharmacological characterization of two compounds in the thienopyrimidine class that are potent, highly selective, and bioavailable small molecule IRAK4 inhibitors for the treatment of autoimmune disorders and B cell malignancies.

RESULTS AND DISCUSSION

Discovery of potent and selective IRAK4 inhibitors

Using a published cocrystal structure of IRAK4 (Wang et al., 2006), we conducted a virtual screen of a commercially available library of 1.3 million compounds. Confirmation of IRAK4 inhibition by several virtual screen hits resulted in the identification of a compound containing a thienopyrimidine motif. Elaboration of this early hit led to the identification of two highly potent and selective IRAK4 inhibitors, ND-2158 and ND-2110, which are competitive inhibitors that bind in the ATP pocket and are built upon novel structural scaffolds (Fig. 1 A). The in vitro inhibitory constants (Ki) versus IRAK4 kinase for ND-2158 and ND-2110 were 1.3 nM and 7.5 nM, respectively (Fig. 1 B). When tested against 334 kinases, these inhibitors were highly selective for IRAK4 (Fig. 1 C and Table S1) and exhibited attractive drug-like properties including solubility, cell permeability, and a pharmacokinetic profile suitable to pharmacologically interrogate IRAK4-dependent mechanisms in cells and animal disease models (Fig. 1 D).

IRAK4 inhibitors block TNF production, collagen-induced arthritis, and gout formation in mice

The importance of TLR signaling in inflammatory cell responses (Kawai et al., 1999; Suzuki et al., 2002; Kim et al., 2007) prompted us to investigate the use of IRAK4 inhibitors in this setting. ND-2158 or ND-2110 potently blocked production of the proinflammatory cytokine TNF by human white blood cells (WBCs) stimulated with the TLR4 agonist LPS or the TLR9 agonist CpG; however, the structurally related compound ND-1659, which does not inhibit IRAK4 kinase activity, was inactive (Fig. 1, A and B; and Fig. 2 A). ND-2158 or ND-2110 also significantly reduced serum TNF levels in a

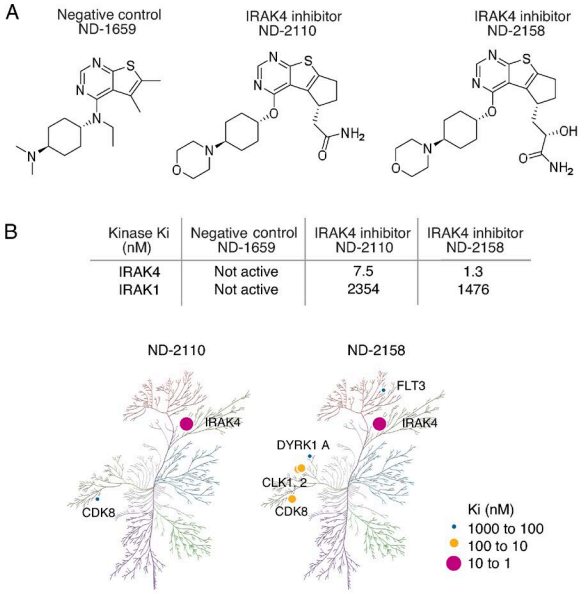

Kinase Ki (nM)	Negative control ND-1659	IRAK4 inhibitor ND-2110	IRAK4 inhibitor ND-2158
IRAK4	Not active	7.5	1.3
IRAK1	Not active	2354	1476

D

Potency and drug-like properties		ND-2110	ND-2158
Cell-based Cytokine production IC_{50} (nM)	THP-1 cells (LPS -> TNF)	613 ± 319	130 ± 50
	WBC (R848 -> TNF)	571	211 ± 158
	Whole blood (R848 -> TNF)	653 ± 240	316 ± 163
In vivo mouse PK	Dosing route	PO	IP
	Dosing level (mg/kg)	10	3
	$T_{1/2}$ (h)	1.4	0.43
	C_{MAX} (μM)	0.21	1.0
	AUC_{last} (μM*h)	0.53	0.98
	% F	23	101
Physical properties	Solubility (μM)	291	>300

Figure 1. **ND-2110 and ND-2158 are highly potent and selective IRAK4 inhibitors.** (A) Structures for IRAK4 inhibitors, ND-2110 and ND-2158, and a negative control compound, ND-1659. (B) Kinome maps showing selectivity of ND-2110 and ND-2158 across 334 kinases. Those kinases with Ki < 1 μM are shown on the kinome maps. (C) Dose–response curves showing inhibition of IRAK4 and IRAK1 kinase activity in the presence of ND-2110 and ND-2158. Percent activity was calculated using the no inhibitor control as 100% activity. Data show a representative experiment from three independent experiments. (D) Cellular potency and pharmacokinetics of ND-2110 and ND-2158. In vivo pharmacokinetic (PK) profiles of ND-2110 and ND-2158 in mice treated with the indicated doses of either IRAK4 inhibitor. Half-life ($T_{1/2}$), maximum serum concentration (C_{max}), area under the curve (AUC) of the drug concentration time profile, and % bioavailability (% F) are shown. R848 refers to the TLR7/8 MYD88-dependent signaling inhibitor.

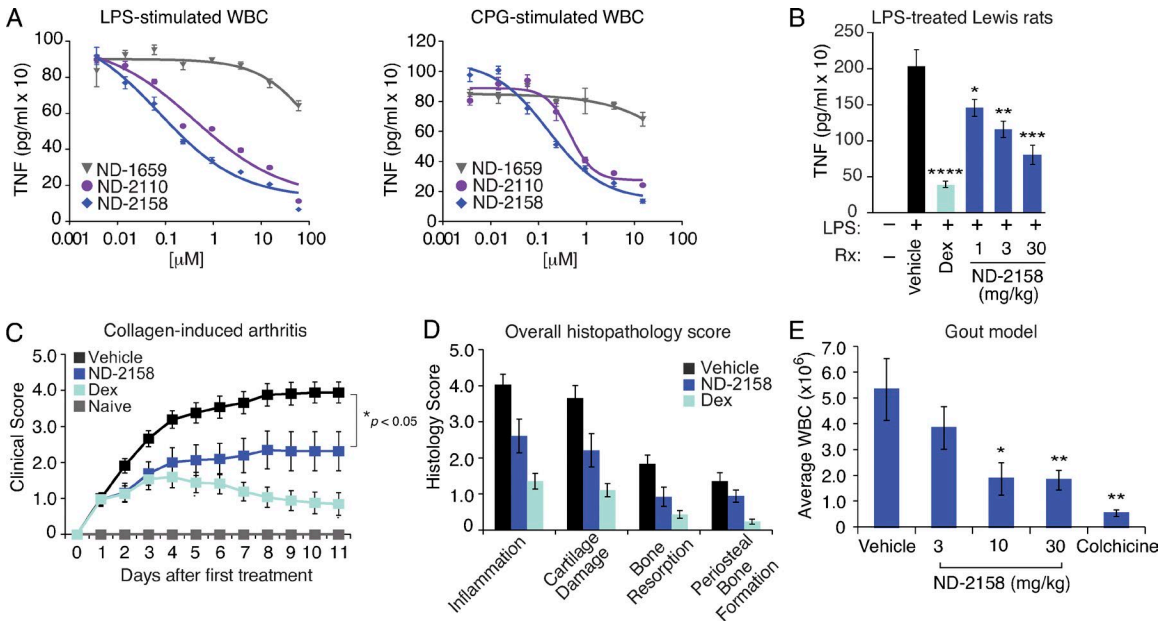

Figure 2. **IRAK4 inhibitors block TNF production, collagen-induced arthritis, and gout formation in mice.** (A) Primary human peripheral WBCs were pretreated with IRAK4 inhibitors ND-2158 (n = 10 experiments) or ND-2110 (n = 2 experiments) for 1 h, followed by stimulation with 1 µg/ml LPS or 0.5 µM CpG. TNF in the cell culture supernatant was assessed by ELISA. ND-1659 (gray line) lacking IRAK4 inhibitory activity was included as a negative control. Data show a representative experiment, and error bars represent SD. (B) Serum TNF from Lewis rats (n = 10 per group) treated with the indicated doses of ND-2158, followed by LPS challenge. Dex served as a positive control. Data show mean ± SEM. *, P < 0.05; **, P < 0.01; ***, P < 0.001; ****, P < 0.0001, Student's t test comparing ND-2158 treatment groups with vehicle control. (C) Male DBA mice (n = 8 per group, except n = 4 naive controls) were immunized with collagen and randomly enrolled at arthritis onset. ND-2158 (30 mg/kg) or Dex treatment (0.1 mg/kg) was initiated on day 1. Mice were evaluated daily for clinical scores. Data indicate mean ± SEM. *, P < 0.05 (days 2–11), Student's t test comparing IRAK4 inhibitor with vehicle treatment. (D) Histological evaluation of overall arthritic clinical scores. Error bars represent SEM. Scores: 0 = normal, 1 = minimal, 2 = mild, 3 = moderate, 4 = marked, 5 = severe. (E) Male BALB/c mice (n = 10 per group) were treated for 6 d with the indicated doses of ND-2158. Inflammation was then induced by MSU injection into the air pouch. Colchicine served as a positive control. Data indicate mean WBC count ± SEM. *, P < 0.05; **, P < 0.01, Student's t test comparing treatment groups with vehicle control.

dose dependent manner in vivo (Fig. 2 B and not depicted). In mouse models of arthritis and inflammatory gout, signaling through the MYD88–IRAK4 complex is required for development of overt disease (Choe et al., 2003; Chen et al., 2006; Ehlers et al., 2006; Pierer et al., 2011). In a collagen-induced arthritis mouse model (Bendele, 2001), pharmacological IRAK4 inhibition was effective within 2 d of initiating treatment (Fig. 2 C, dark blue squares). Inflammation reduction was examined by histological evaluation of inflammatory cell influx, cartilage damage, bone resorption, and periosteal bone formation (Fig. 2 D). In a mouse model of MYD88-dependent inflammatory gout (Chen et al., 2006), IRAK4 inhibition blocked leukocyte infiltration in a dose-dependent manner, with the higher doses achieving more than twofold reduction in leukocyte influx compared with vehicle control (Fig. 2 E). Together, our data demonstrate that these IRAK4 inhibitors can interrupt IRAK4-dependent responses in vitro and in vivo.

Pharmacological IRAK4 inhibition in *MYD88* L265P–expressing ABC DLBCL

Activating oncogenic mutations in *MYD88*, particularly the L265P variant, are pathognomonic for ABC DLBCL (Ngo et al., 2011), leading us to explore the activity of small molecule IRAK4-selective inhibitors in this malignancy. The in vitro viability of multiple ABC DLBCL lines was reduced by ND-2158 and ND-2110, but not the control compound ND-1659, whereas GCB DLBCL lines with WT *MYD88* were unaffected (Fig. 3 A and not depicted). ND-2158 and ND-2110 targeted the subset of ABC DLBCL lines with *MYD88* L265P mutations, but not ABC DLBCL lines with other *MYD88* mutations (S222R and S219C) or those with WT *MYD88* (Fig. 3 A and not depicted). In a mouse xenograft model created using the ABC DLBCL line OCI-Ly10 (MYD88 L265P+), the IRAK4 inhibitor ND-2158 retarded tumor growth and was well tolerated (Fig. 3, B and C) and reduced IRAK4 phosphorylation (Thr-345/Ser-346) in the tumors (Fig. 3 D).

Effect of IRAK4 inhibitors on oncogenic MYD88 signaling in ABC DLBCL

IRAK4 phosphorylates three residues within its activation loop: Thr-342, Thr-345, and Ser-346 (Cheng et al., 2007). This autophosphorylation event is the first step required for IRAK4 activation and leads to IRAK1 phosphorylation and the constitutive NF-κB signaling that sustains ABC DLB

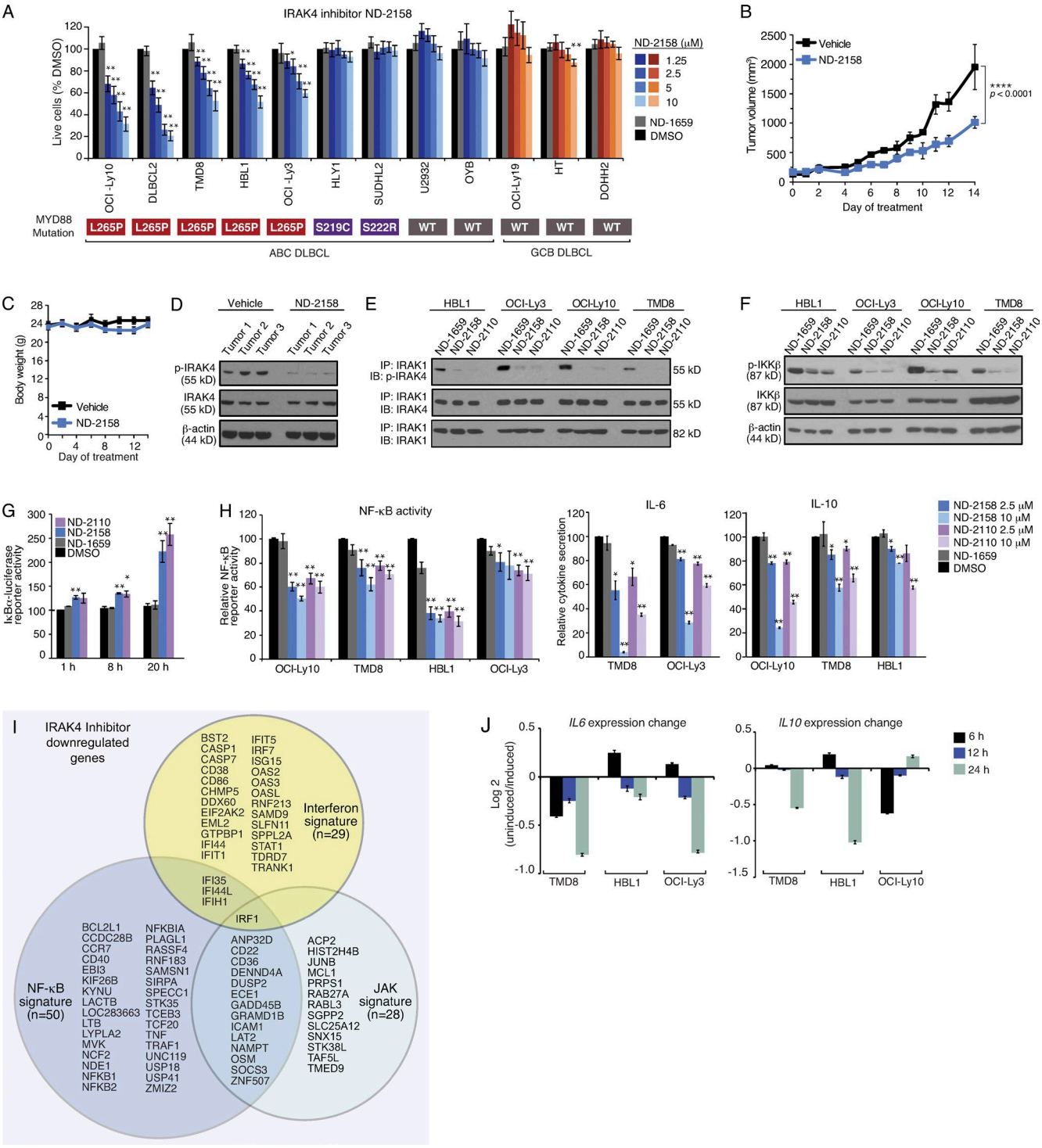

Figure 3. **Selective activity of IRAK4 inhibitors against ABC DLBCL.** (A) Viability (MTS assay) of DLBCL lines after 4-d treatment with the indicated concentrations of ND-2158, normalized to control (DMSO)-treated cells. Data represent mean ± SEM from eight independent experiments. *, P < 0.05; **, P < 0.01, Student's *t* test comparing treatment groups with DMSO control. (B) Efficacy of the IRAK4 inhibitor ND-2158 on ABC DLBCL growth in vivo. NOD/SCID mice ($n = 4$ per treatment group) bearing ABC DLBCL OCI-Ly10 tumors were treated with ND-2158 (100 mg/kg/day; twice daily). Tumor growth was measured as a function of tumor volume. Data show mean ± SEM per treatment group. ****, P < 0.0001, calculated using a mixed effects model to test the interaction between growth rate and treatment. (C) Body weight analysis of NOD/SCID mice ($n = 4$ per treatment group) bearing OCI-Ly10 ABC DLBCL tumors and treated with ND-2158 for 14 d (100 mg/kg/day; twice daily). Data show mean body weight ± SEM. (D) NOD/SCID mice bearing OCI-Ly10 ABC DLBCL tumors were treated for 3 d with either ND-2158 (100 mg/kg/day; twice daily) or vehicle. 2 h after final dosing, tumors were examined by immunoblotting for p-IRAK4,

CL survival (Cheng et al., 2007; Ngo et al., 2011; Ferrao et al., 2014). When we treated ABC DLBCL lines (MYD88 L265P+) with ND-2158, ND-2110, or the negative control compound ND-1659, coimmunoprecipitation analysis revealed that IRAK4 associates with IRAK1 and is autophosphorylated in this complex (Fig. 3 E). Pretreatment of cells with IRAK4 inhibitors decreased the level of IRAK4 autophosphorylation (Thr-345/Ser-346) relative to cells treated with the inactive compound ND-1659 (Fig. 3 E).

Oncogenic MYD88 signaling engages the NF-κB pathway by activating IκB kinase β (IKKβ)–mediated phosphorylation and degradation of IκB proteins (Ngo et al., 2011). Treatment of ABC DLBCL lines with the IRAK4 inhibitors suppressed IKK activation, as indicated by decreased phosphorylation of IKKβ (Fig. 3 F), and stabilization of an IκBα-luciferase reporter, which measures IKK activity (Fig. 3 G; Lam et al., 2005). Moreover, in four MYD88 L265P+ ABC DLB CL lines, ND-2158 or ND-2110 decreased transcription of an NF-κB–dependent luciferase reporter (Fig. 3 H) and reduced secretion of IL-6 and IL-10 (Fig. 3 H), two cytokines that depend on MYD88-mediated NF-κB activation for their production (Ngo et al., 2011).

To explore the biological consequences of inhibiting IRAK4 activity in ABC DLBCL, we profiled gene expression changes over time in four MYD88 L265P+ ABC DLBCL lines treated with ND-2158 or the negative control ND-1659. We defined an IRAK4 gene expression signature consisting of 366 down-modulated genes, which was highly enriched for genes whose expression depends on *MYD88* activity (Fig. 3 I and Table S2; sevenfold enrichment, $P = 2.3 \times 10^{-21}$; Ngo et al., 2011). When the overlap between the IRAK4 signature and previously defined gene expression signatures was examined, the most significant enrichment was with signatures reflecting NF-κB signaling (Fig. 3 I and Fig. S1 and Table S2; 13-fold enrichment, $P = 5.3 \times 10^{-40}$).

Autocrine IL-6 and IL-10 production in ABC DLBCL drives JAK–STAT3 signaling and promotes ABC DLBCL survival (Lam et al., 2008). ND-2158 reduced gene expression of *IL6* and *IL10* (Fig. 3 J), and accordingly, a signature of JAK kinase signaling in ABC DLBCL overlapped significantly with the IRAK4 signature (Fig. 3 I, Fig. S1, and Table S2; fivefold enrichment, $P = 1.7 \times 10^{-11}$). MYD88 signaling also induces IFN-β production in ABC DLBCL cells (Ngo et al., 2011; Yang et al., 2012), and a subset of genes induced by type I IFN signaling were also components of the IRAK4 signature (Fig. 3 I, Fig. S1, and Table S2; fivefold enrichment, $P = 7.2 \times 10^{-13}$). Thus, pharmacological IRAK4 inhibition blunts multiple biological responses downstream of oncogenic MYD88 signaling in ABC DLBCL.

Combined inhibition of oncogenic MYD88 and BCR signaling

Bruton's tyrosine kinase (BTK) is a promising therapeutic target in ABC DLBCL (Wilson et al., 2015). BTK is a crucial kinase linking proximal BCR signaling to downstream IKK activation and maintains NF-κB activity (Davis et al., 2010). In many ABC DLBCL lines, both chronic active BCR signaling and constitutive MYD88 signaling converge on IKK, suggesting that dual inhibition of these two pathways could have synergistic effects on ABC DLBCL killing. Combination of the BTK inhibitor ibrutinib with ND-2158 enhanced killing of BCR-dependent ABC DLBCL that harbor coincident MYD88 L265P mutations and activating mutations in the BCR subunits CD79A and CD79B (OCI-Ly10 and TMD8). In contrast, no increased killing was observed for a GCB DLB CL line (OCI-Ly19) that does not rely on either MYD88 or BCR signaling (Fig. 4 A). Isobologram analysis confirmed that ND-2158 and ibrutinib were synergistic (Fig. 4, B and C). The combination was also more effective in inhibiting IKK activity (Fig. 4 D) and enhancing apoptosis (Fig. 4 E). ND-2158 and ibrutinib also cooperated to suppress the in vivo growth of OCI-Ly10 xenografts (Fig. 4 F), laying the foundation for combined use of ibrutinib and IRAK4 inhibitors in future clinical trials.

A subset of ABC DLBCLs with chronic active BCR signaling require spleen tyrosine kinase (Syk) to deliver signals from the BCR to downstream survival pathways, including NF-κB and PI(3) kinase (Davis et al., 2010). ND-2158 and the selective Syk inhibitor PRT062607 (Coffey et al., 2012) were synergistic in killing ABC DLBCL lines that depend on both BCR and MYD88 signaling (OCI-Ly10,

IRAK4 (total), and β-actin. Data show the individual tumor from three separate mice per treatment group. (E) ABC DLBCL lines were treated for 4 h with 10 µM ND-2158, ND-2110, or negative control compound ND-1659. Anti-IRAK1 immunoprecipitates were examined by immunoblotting for phosphorylated IRAK4, IRAK4 (total), and IRAK1 (total). Data are representative of three independent experiments. (F) Immunoblots for phosphorylated IKKβ, total IKKβ, and β-actin in ABC DLBCL lines treated for 4 h with 10 µM ND-2158, ND-2110, or negative control compound ND-1659. Data are representative of three independent experiments. (G) Relative activity of an IκBα-dependent luciferase reporter in TMD8 cells (ABC DLBCL) after treatment with 10 µM ND-2158, ND-2110, or negative control compound ND-1659 for the indicated time periods. Data show mean ± SEM from three independent experiments. *, $P < 0.05$; **, $P < 0.01$, Student's *t* test comparing treatment groups with DMSO control. (H, left) NF-κB–dependent luciferase activity in ABC DLBCL lines treated for 20 h with ND-2158, ND-2110, negative control compound ND-1659, or DMSO. Data indicate mean ± SEM from four independent experiments. (middle and right) Secretion of IL-6 or IL-10 from ABC DLBCL lines treated for 48 h with ND-2158, ND-2110, negative control compound ND-1659, or DMSO. Data show a representative experiment from at least four independent experiments. Data indicate mean ± SD. *, $P < 0.05$; **, $P < 0.01$, Student's *t* test comparing treatment groups with DMSO control. (I) Venn diagram of genes down-modulated over a time course of 10 µM ND-2158 treatment (6, 12, and 24 h) in four ABC DLBCL lines (see Materials and methods). Genes are grouped according to membership in gene expression signatures. (J) Gene expression change in *IL6* or *IL10* over a time course of ND-2158 treatment. ABC DLBCL lines were treated for 0, 6, 12, or 24 h with either 10 µM ND-2158 or 10 µM of negative control compound ND-1659. Data were normalized to ND-1659 treatment and indicate mean ± SD of 10 replicates.

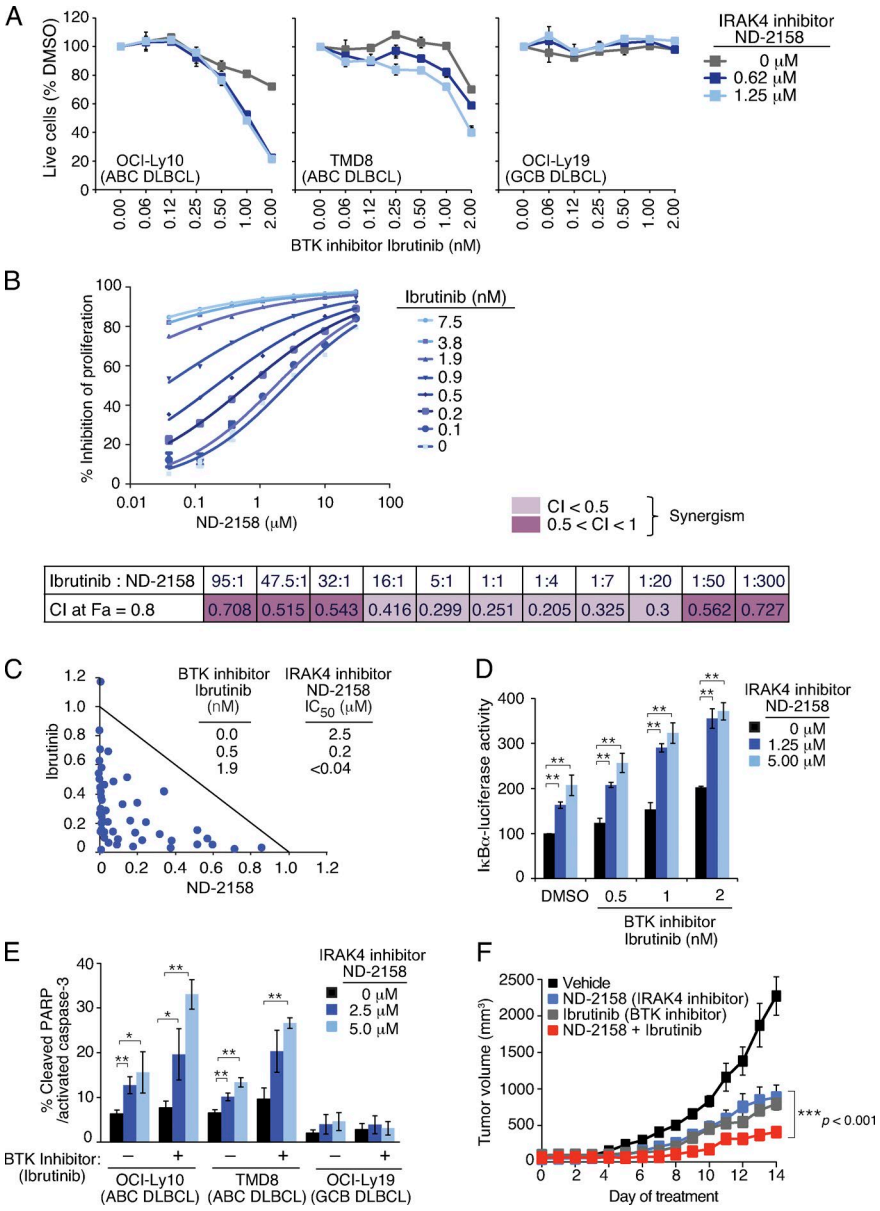

Ibrutinib : ND-2158	95:1	47.5:1	32:1	16:1	5:1	1:1	1:4	1:7	1:20	1:50	1:300
CI at Fa = 0.8	0.708	0.515	0.543	0.416	0.299	0.251	0.205	0.325	0.3	0.562	0.727

Figure 4. **Pharmacological IRAK4 inhibition synergizes with BTK inhibition to promote killing of ABC DLBCL.** (A) Viability (MTS assay) of DLBCL lines after 4-d treatment with ND-2158, ibrutinib, or both. Data were normalized to DMSO-treated cells and then to cells treated with ND-2158 alone. Data indicate mean ± SEM of triplicates. (B) OCI-Ly10 cells were treated for 4 d with the indicated doses of ND-2158 plus ibrutinib, followed by MTS assay. CI and Fa were obtained using the software package CalcuSyn (see Materials and methods). Dose ratio for the combinations resulting in synergism (CI < 1) at the 80% effect (Fa = 0.8) is shown in the table. CI values of <0.5 are shown in light pink and between 0.5 and 1 are shown in dark pink. Drug synergism, addition, and antagonism are defined by CI values of <1.0, 1.0, and >1.0, respectively. (C) CalcuSyn plotted isobologram for the synergistic effect on ABC DLBCL viability when combining ND-2158 plus ibrutinib. OCI-Ly10 cells were cultured with ibrutinib (twofold dilution starting at 7.5 nM to 0.1 nM), ND-2158 (fourfold dilution starting at 30 μM to 0.12 μM), or both for 4 d, followed by MTS assay. The table shows the shift in ND-2158 IC_{50} in the presence of the respective concentrations of ibrutinib. (D) Relative IκBα luciferase activity in TMD8 cells treated overnight with the indicated concentrations of ibrutinib, in combination with either DMSO or ND-2158. Data show mean ± SEM from three independent experiments. **, P < 0.01, Student's *t* test. (E) DLBCL lines were treated with ND-2158, 1 nM ibrutinib, or both for 72 h. Apoptotic cells were measured by FACS for the percentage of cells double-positive for cleaved PARP and activated caspase-3. Data show mean ± SEM of five independent experiments. *, P < 0.05; **, P < 0.01, Student's *t* test. (F) NOD/SCID mice (n = 4 per treatment group) bearing OCI-Ly10 ABC DLBCL tumors were treated with ND-2158 (100 mg/kg/day; twice daily), ibrutinib (9 mg/kg/day; once daily), or a combination of ND-2158 plus ibrutinib. Data show mean tumor volume ± SEM. ***, P < 0.001 comparing ND-2158 treatment alone with combination ND-2158 plus ibrutinib treatment. P-values were calculated using a mixed effects model to test the interaction between growth rate and treatment.

TMD8, and HBL1), but a control GCB DLBCL line was unaffected (Fig. 5, A–C). The observed cytotoxicity was associated with increased apoptosis and decreased IKK activity in cells treated with the combination compared with either drug alone (Fig. 5, D and E).

Combined inhibition of MYD88 and Bcl-2 signaling in ABC DLBCL

The antiapoptotic protein Bcl-2 provides a powerful survival signal in ABC DLBCL and is characteristically expressed at high levels as the result of transcriptional up-regulation and amplification of the *BCL2* locus (Alizadeh et al., 2000; Lenz et al., 2008). The Bcl-2 inhibitor ABT-199 synergistically enhanced the ability of ND-2158 to decrease viability of ABC DLBCL lines (Fig. 6 A) and promote apoptosis, as indicated by more cells expressing activated caspase-3 and cleaved PARP (Fig. 6 B). Of note, this synergy was observed in the CARD11 mutant ABC line OCI-Ly3 that does not rely on BCR signaling and is insensitive to ibrutinib (Fig. 6 A; Davis et al., 2010). In vivo, ND-2158 or

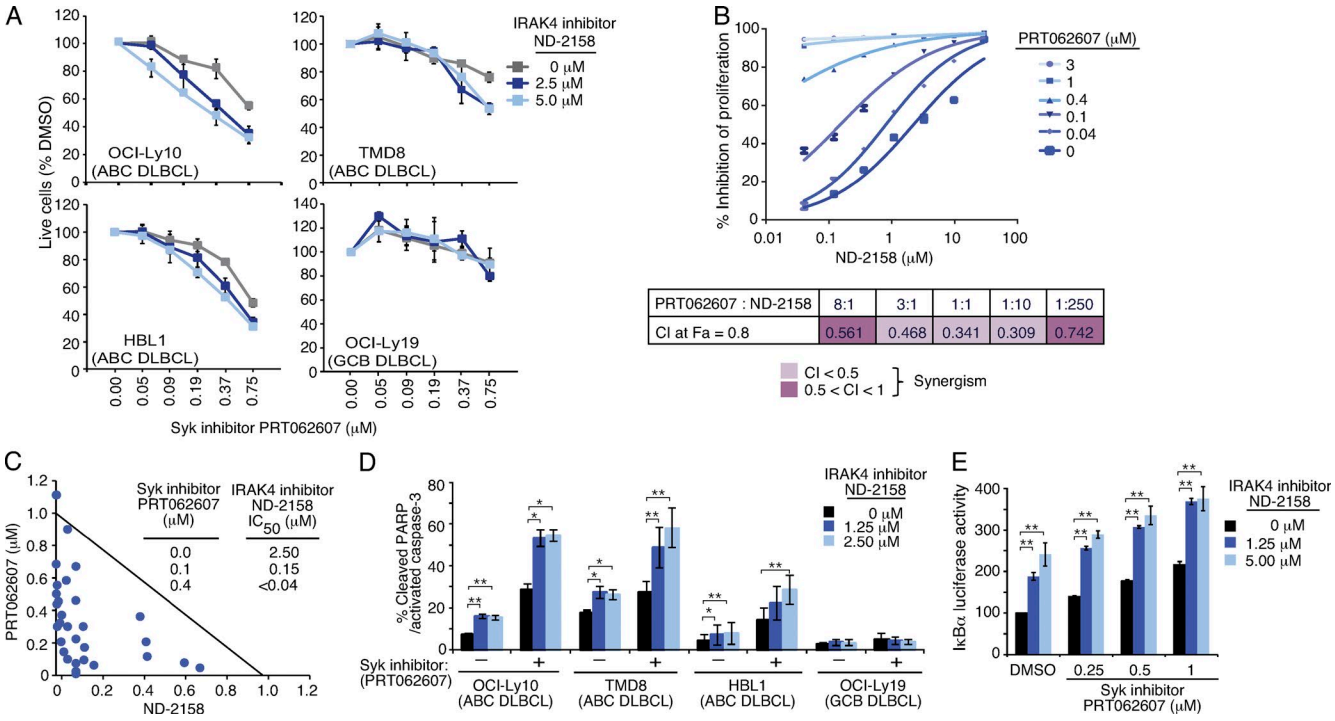

Figure 5. **Pharmacological IRAK4 inhibition synergizes with Syk inhibition to promote killing of ABC DLBCL.** (A) Viability (MTS assay) of DLBCL lines after 4-d treatment with ND-2158, PRT062607, or both. Data were normalized to DMSO-treated cells and then to cells treated with ND-2158 alone. Data indicate mean ± SEM of triplicates. (B) OCI-Ly10 cells were treated for 4 d with the indicated doses of ND-2158 plus PRT062607, followed by MTS assay. CI and Fa were obtained using the software package CalcuSyn (see Materials and methods). Dose ratio for the combinations resulting in synergism (CI < 1) at the 80% effect (Fa = 0.8) are shown in the table. CI values of <0.5 are shown in light pink and between 0.5 and 1 are shown in dark pink. Drug synergism, addition, and antagonism are defined by CI values of <1.0, 1.0, and >1.0, respectively. (C) CalcuSyn plotted isobologram for the synergistic effect on ABC DLBCL viability when combining ND-2158 plus PRT062607. OCI-Ly10 cells were cultured with PRT062607 (threefold dilution starting at 3 μM to 0.04 μM), ND-2158 (threefold dilution starting at 30 μM to 0.04 μM), or both together for 4 d, followed by MTS assay. The table shows the shift in ND-2158 IC_{50} in the presence of the respective concentrations of PRT062607. (D) DLBCL lines were treated with the indicated concentrations of ND-2158, 1 μM PRT062607, or both for 72 h. Apoptotic cells were measured by FACS for the percentage of cells double positive for cleaved PARP and activated caspase-3. Data show mean ± SEM of eight independent experiments. *, P < 0.05; **, P < 0.01, Student's *t* test. (E) Relative IκBα luciferase activity in TMD8 cells (ABC DLBCL) treated overnight with PRT062607, in combination with either DMSO or ND-2158 at the indicated concentrations. Data show mean ± SEM from three independent experiments. **, P < 0.01, Student's *t* test.

ABT-199 moderately suppressed growth of OCI-Ly3 xenografts as single agents, but together they produced near complete inhibition of tumor growth (Fig. 6 C). In addition to Bcl-2, ABC DLBCLs express three other antiapoptotic Bcl-2 family members: *BCL2L1*, *MCL1*, and *BCL2A1* (encoding Bcl-x_L, Mcl-1, and A1, respectively). The IRAK4 inhibitor ND-2158 decreased *BCL2L1* and *BCL2A1* mRNA levels but increased *BCL2* expression (Fig. 6 D), suggesting that the synergy between ND-2158 and ABT-199 could be caused by combined inhibition of all three family members (Bcl-x_L, A1, and Bcl-2).

In summary, the potent and selective IRAK4 kinase inhibitors reported here provide insights into disease mechanisms and suggest new therapeutic strategies for patients with inflammatory diseases and B cell malignancies. Recently, two papers have been published that describe IRAK4 inhibitors with in vivo efficacy in LPS-induced TNF models and in an antibody-induced mouse arthritis model of inflammation (Tumey et al., 2014; McElroy et al., 2015). The compounds described by Tumey et al. (2014) are flat tetracyclic aromatic compounds that possess high protein binding (>99%), low permeability, and high efflux, which is reflected in poor oral bioavailability. McElroy et al. (2015) describe an amidopyrazole IRAK4 inhibitor with good solubility and modest protein binding, which exhibits paw size reduction in a mouse model of arthritis. However, a subsequent publication by the same group (Lim et al., 2015) describes the difficulty in obtaining desired drug-like properties (selectivity, permeability, and cell potency) in this series of compounds. In contrast, our thienopyrimidine compounds described herein possess excellent selectivity and solubility, low protein binding, good permeability and cell potency, and in vivo activity in several autoimmune and tumor efficacy models.

Despite the advent of anti-TNF biologics and JAK kinase inhibitors, many patients with autoimmune or chronic inflammatory diseases must still be treated with broad-acting immunosup-

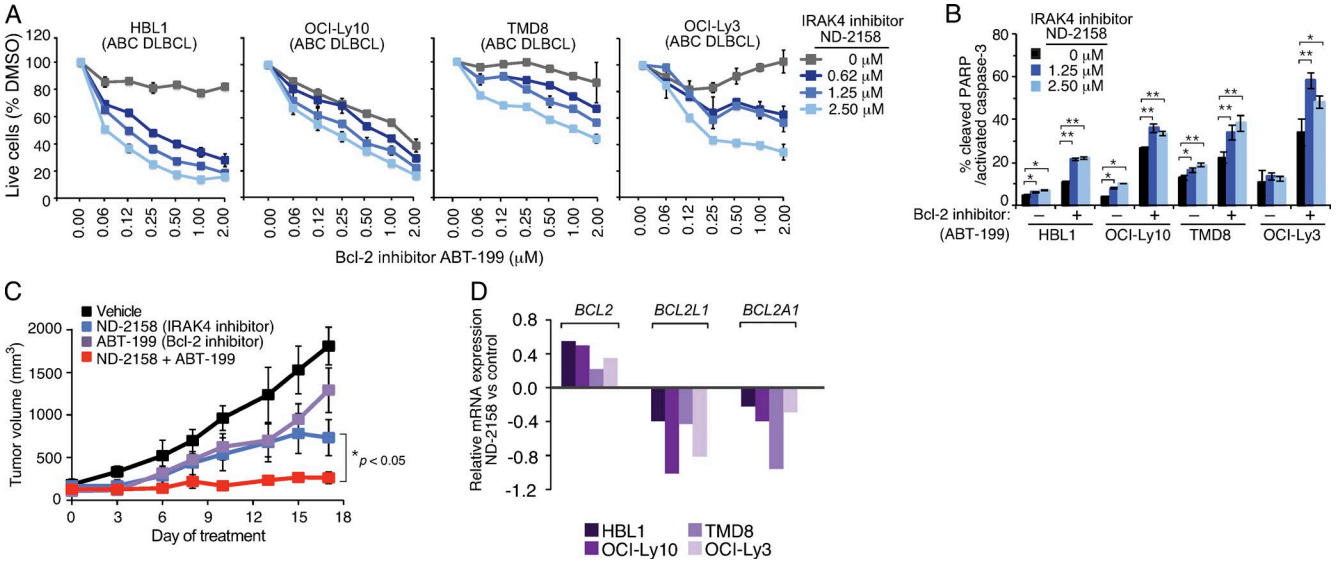

Figure 6. **Pharmacological IRAK4 inhibition synergizes with the Bcl-2 inhibitor ABT-199 to promote killing of ABC DLBCL.** (A) Viability (MTS assay) of ABC DLBCL lines after 4-d treatment with ND-2158, ABT-199, or ND-2158 plus ABT-199. Data were normalized to DMSO-treated cells and then to cells treated with ND-2158 alone. Data indicate mean ± SEM of triplicates. (B) ABC DLBCL lines were treated with the indicated concentrations of ND-2158, 1 μM ABT-199, or both for 72 h. Apoptotic cells were measured by FACS for the percentage of cells double positive for cleaved PARP and activated caspase-3. Data indicate mean ± SEM of triplicates. *, P < 0.05; **, P < 0.01, Student's *t* test. (C) NOD/SCID mice ($n = 4$ per treatment group) bearing OCI-Ly3 ABC DLBCL tumors were treated with ND-2158 (100 mg/kg/day; twice daily), ABT-199 (50 mg/kg/day; once daily), or a combination of ND-2158 plus ABT-199. Each point on the graph indicates the mean tumor volume ± SEM. *, P < 0.05 comparing ND-2158 treatment alone with combination ND-2158 plus ABT-199 treatment. P-values were calculated using a mixed effects model to test the interaction between growth rate and treatment. (D) ABC DLBCL lines were treated for 24 h with either 10 μM ND-2158 or 10 μM of negative control compound ND-1659. Gene expression change in antiapoptotic *BCL2* family genes from 0 to 24 h is shown. Data were normalized to treatment with the negative control compound ND-1659.

pressive agents. We have shown that pharmacological inhibition of IRAK4 ameliorates clinical progression of collagen-induced arthritis and blocks gout formation in mouse models.

Among mature B cell malignancies, mutations affecting *MYD88* have emerged as one of the most prevalent gain-of-function genetic alterations. Our work establishes that oncogenic MYD88 signaling is a tractable therapeutic target in human lymphomas and supports the development of IRAK4 inhibitors for treatment of the genetically defined subset of ABC DLBCL harboring the *MYD88* L265P mutation. Our systematic exploration of small molecule combinations also revealed the value of IRAK4 blockade in enhancing the efficacy of small molecules that target orthogonal ABC DLBCL survival pathways. Thus, IRAK4 inhibitors may have clinical utility in ABC DLBCL, either alone or in combination with pharmacological blockade of the BCR or Bcl-2 pathways. The therapeutic potential of IRAK4 inhibitors may also extend beyond ABC DLBCLs because *MYD88* L265P is prevalent in multiple mature B cell lymphoma subtypes, including Waldenström's macroglobulinemia (91%; Treon et al., 2012), primary central nervous system lymphoma (75%; Kraan et al., 2013), primary cutaneous DLBCL–leg type (69%; Pham-Ledard et al., 2012), primary testicular DLBCL (68%; Kraan et al., 2014), MALT lymphoma (6%; Ngo et al., 2011; Li et al., 2012), and chronic lymphocytic leukemia (3%; Puente et al., 2011).

MATERIALS AND METHODS

Reagents

Synthesis of ND-2158 and ND-2110 (examples 106 and 29) has been reported previously (Corin et al., 2012).

Kinase assays

Kinase activity was evaluated using radioisotope-based enzymatic assays, and the experiments were conducted at Reaction Biology Corp. (Ma et al., 2006). IC_{50} and Ki of ND-2158 and ND-2110 were obtained in dose inhibition assays against IRAK4 and IRAK1. Broad kinase selectivity was evaluated against 334 kinases at one concentration (10 μM) of ND-2158 or ND-2110. IC_{50} and Ki were subsequently determined for kinases that showed ≥75% inhibition at 10 μM of the compounds. Dose–response curves were generated with Prism software (GraphPad Software) using four-parameter fit.

In vitro solubility of ND-2110 and ND-2158

300 μM of either ND-2110 or ND-2158 was prepared in Dulbecco's phosphate-buffered saline (D-PBS), pH 7.4, containing 0.1% DMSO. Samples were incubated at 25°C for 2 h with shaking using a plate shaker. At the end of the incubation, samples were filtered, the filtrate was diluted 100-fold with methanol, and the drug level was determined using the API 4000 Q TRAP LC/MS/MS system (Applied Biosystems).

Cell lines

DLBCL cell lines were cultured in RPMI 1640 medium (Gibco) supplemented with penicillin/streptomycin (Gibco) and 20% fetal bovine serum. For the OCI series of DLBCL cell lines, Iscove's medium supplemented with 100 U/ml penicillin/streptomycin and 20% fresh human plasma was used. Cells were propagated in humidified, 5% CO_2 incubators at 37°C. THP-1 cells from ATCC (TIB-202) were cultured in THP-1 media containing RPMI 1640, 10% fetal bovine serum, 100 U/ml penicillin/streptomycin, and 50 μM 2-Mercaptoethanol (Invitrogen).

LPS, CpG, and R848–induced cytokine release

Human WBCs were isolated from the Buffy coat by lysing red blood cells. Cells were preincubated for 1 h with ND-2158, ND-2110, or ND-1659 at concentrations shown in Fig. 2 A, with a final concentration of 0.3% DMSO, before stimulation with the indicated agonists. WBCs were plated in RPMI 1640 containing 100 U/ml penicillin/streptomycin and stimulated with 1 μg/ml LPS (InvivoGen), 0.5 μM CpG (InvivoGen), or 1 μM of the TLR7/8 inhibitor R848 (InvivoGen) for 20 h (Jurk et al., 2011; Matera et al., 2012). For R848-induced cytokine release assays (Fig. 1 D), human whole blood was collected in sodium heparin vacutainer tubes and diluted with an equal volume of RPMI 1640 for 30 min. Blood was then stimulated with 1 μM R848 for 20 h, and plasma was collected at the end of stimulation for TNF analysis. THP-1 cells were plated in THP-1 media (RPMI 1640, 10% fetal bovine serum,100 U/ml penicillin/streptomycin, and 50 μM 2-Mercaptoethanol) and stimulated with 300 ng/ml LPS for 5 h. All assays were performed in 96-well plates. TNF production in the WBC culture supernatant or human whole blood was detected using the TNF ELISA kit (R&D Systems). TNF production in the THP-1 cell supernatant (Fig. 1 D) was detected using the TNF HTRF kit (Cisbio), as per manufacturer instructions.

Gene expression array and gene expression signature enrichment

Four ABC DLBCL cell lines (OCI-Ly10, TMD8, HBL1, and OCI-Ly3), were treated with either 10 μM ND-2158 or 10 μM of the structurally related negative control compound ND-1659 for 6, 12, 24, or 36 h in culture. Cells were harvested at each time point, and RNA for gene expression was prepared from 5 million cells using TRIzol (Invitrogen) extraction, followed by clean up using the RNeasy kit (QIA GEN). Gene expression profiling was performed using two-color human Agilent 4 × 44K gene expression arrays (Agilent Technologies), as described by the manufacturer, comparing signal from control compound-treated (ND-1659) control cells (Cy3) with cells treated with ND-2158 (Cy5) for the indicated times. Array elements were filtered for those meeting confidence thresholds for spot size, architecture, and level above local background. These criteria are a feature of the Agilent Technologies gene expression software package for Agilent 4 × 44K arrays. Gene expression signature enrichment was performed by comparing changes in gene expression from at least two ABC DLBCL cell lines, occurring in at least two time points after ND-2158 treatment. Gene expression signature enrichment analysis was performed as described previously (Yang et al., 2012). Gene expression data has been deposited under GEO accession no. GSE63029.

NF-κB and IκBα reporter assays

The generation of stable NF-κB firefly luciferase reporter ABC DLBCL lines (OCI-Ly10, TMD8, HBL1, and OCI-Ly3) has previously been described (Ceribelli et al., 2014). For drug response experiments, cells were seeded at a density of 2.5×10^5 cells per ml in 96-well plates. Cells were treated with drugs for the indicated times (as described in the figure legends). Firefly luciferase and Renilla activity was measured using the Dual-Glo Luciferase Reporter Assay System (Promega) according to the manufacturer's protocol. Luminescence from equivalent amounts of lysate was read in triplicate on a Microtiter Plate Luminometer (Dyn-Ex Technologies). Relative NF-κB activity was determined by normalizing titers of firefly to Renilla luciferase. Generation of the IκBα photinus-luciferase reporter cell line has been described previously (Lam et al., 2005). Relative IκBα activity was determined by normalizing titers of firefly to Renilla luciferase.

Immunoblotting and coimmunoprecipitation

Cells were lysed in an endogenous lysis buffer (20 mM Tris-HCl, pH 7.6, 150 mM NaCl, 1 mM EDTA, 1% Triton X-100, 30 mM NaF, and 2 mM sodium pyrophosphate) supplemented with complete protease inhibitor cocktail (Roche), phosphatase inhibitor tablet (Roche), 1 mM DTT, 1 mM Na_3VaO_4, and 1 mM PMSF. Samples were cleared by centrifugation at 14,000 rpm, and protein concentration was measured using the BCA Protein Assay kit (Thermo Fisher Scientific). For immunoblotting, total proteins were separated on 4–12% SDS–polyacrylamide gels and transferred to nitrocellulose membranes. For immunoprecipitation experiments, samples were first precleared with Protein G Dynabeads (Invitrogen) for 60 min. Cleared lysates were incubated overnight with an anti-IRAK1 antibody (Santa Cruz Biotechnology, Inc.), followed by Protein G Dynabeads for an additional 2 h at 4°C. Immunoprecipitates were washed five times with 0.5 M NaCl lysis buffer, separated by SDS-PAGE, transferred to nitrocellulose, and analyzed by immunoblotting. Antibodies used were as follows: anti-IKKβ, anti–phospho-IKKβ, anti–phospho-IRAK4 (pThr-345/Ser-346), and anti-IRAK4 (total) from Cell Signaling Technologies; and anti–β-actin and anti-IRAK1 from Santa Cruz Biotechnology, Inc. Secondary HRP-conjugated antibodies were obtained from GE Healthcare.

MTS viability assay

Approximately 10^4 cells (per well) of each DLBCL cell line were cultured in triplicate in a 96-well plate, in the presence

of vehicle (DMSO) or the indicated drugs on day 0. On day 2, each well was replenished with freshly prepared vehicle or drugs dissolved in culture medium. On day 4, cell viability was assayed by adding 20 µl/well of 3-(4,5-dimethylthiazol-2-yl)-5-(3-carboxymethoxyphenyl)-2-(4-sulphophenyl)-2H tetrazolium and an electron coupling reagent (phenazine methosulphate; Promega) and incubating at 37°C for 2 h. Cell viability was determined by measuring the absorbance at 490 nm using a 96-well plate reader. The background was subtracted using a medium-only control. For single agent drug response experiments, the data were normalized to DMSO-treated cells. For combination drug response experiments, data were first normalized to DMSO-treated cells and then to cells treated with the IRAK4 inhibitor ND-2158 alone. A shift of the drug combination curves to the left indicates a more than additive effect of the combination.

Measurement of apoptosis

The activation of apoptosis was measured by intracellular flow cytometry methods (Sciammas et al., 2006). DLBCL lines were cultured for 72 h in the presence of the indicated drugs. Apoptosis was measured by intracellular FACS for activated caspase-3 and cleaved PARP. Apoptotic cells were defined as the percentage of cells double-positive for activated caspase-3 and cleaved PARP. Antibodies used were as follows: anti–active caspase-3 (PE; BD) and anti–cleaved PARP (Asp-214; Alexa Fluor 647; BD), according to the manufacturer's instructions.

IL-6 and IL-10 ELISA

Cytokine measurement was performed on ABC DLBCL lines cultured for 48 h with ND-2158, ND-2110, ND-1659, or vehicle (DMSO) control. The concentration of IL-6 in cell culture supernatants was measured using the BD OptEIA human IL-6 ELISA kit (BD). The concentration of IL-10 in cell culture supernatants was measured using the BD OptEIA human IL-10 ELISA kit (BD), according to the manufacturer's protocol. Each experiment was performed in triplicate.

CalcuSyn and isobologram analysis

A crossover dose response grid was set up to measure cell viability effects of drug combinations. Combination index (CI) and fraction affected (Fa) for each dose combination was calculated from the experimental data by using the software package CalcuSyn (Biosoft). Drug synergism, addition, and antagonism are defined by CI values of <1.0, 1.0, and >1.0, respectively. Fa represents the inhibitory effect for each combination. Normalized isobolograms were generated to describe combined drug effect. Each isobologram contains a line defining additively, adopted to distinguish synergistic and antagonistic interactions of the drug combinations (Chou, 2010).

Statistical analysis

Prism 6 software (GraphPad Software) was used for statistical analysis of data, except for tumor xenograft experiments, which were analyzed using Spotfire S+ 8.2 (TIBCO Software Inc.). For tumor xenograft drug efficacy experiments, tumor volume was modeled using a mixed effects model, assuming a linear relationship between time and log tumor volume, with individual mice representing random effects. P-values represent the significance of the time and treatment interaction term on tumor volume.

Mouse models

Mouse pharmacokinetic analysis. Pharmacokinetic experiments for ND-2110 were performed by dosing DBA1 mice either i.v. at 3 mg/kg in 10% 2-hydroxypropyl-β-cyclodextrin, or by oral gavage at 10 mg/kg in 0.5% methylcellulose. Blood was collected into sodium heparin tubes before dose and at 0.083, 0.25, 0.5, 1, 2, 4, 6, and 8 h after dosing for the i.v. administration arm or 0.25, 0.5, 1, 2, 4, 6, and 8 h after dosing for the oral gavage administration arm. Plasma was prepared and ND-2110 level was quantified by LC/MS/MS with API 5000 Triple Quadropole System (Applied Biosystems). Pharmacokinetic experiments for ND-2158 were performed by dosing male C57BL/6 mice either i.v. or i.p. at 3 mg/kg in 10% 2-hydroxypropyl-β-cyclodextrin. Blood was collected into sodium heparin tubes before dose and at 0.083, 0.25, 0.5, 1, 2, 4, 6, 8, 12, and 24 h after dosing. Plasma was prepared and ND-2158 level was quantified by LC/MS/MS using the API 4000 Q TRAP system (Applied Biosystems). Pharmacokinetic parameters were calculated using Phoenix WinNonlin.

Tumor xenograft models. All animal experiments were performed in accordance with the National Cancer Institute/National Institutes of Health Animal Care and Use Committee (NCI ACUC) guidelines and approval. Female NOD/SCID mice (6–8 wk of age) were inoculated by s.c. injection of a tumor cell suspension containing Matrigel (Matrigel Basement Membrane Matrix; BD)/PBS at a ratio of 1:1. For the OCI-Ly10 ABC DLBCL line, 10×10^6 cells were inoculated. For the OCI-Ly3 ABC DLBCL line, 10^6 cells were inoculated. Mice were monitored daily for palpable tumor mass. When tumors reached a mean of 150 mm^3, treatment was initiated. ND-2158 was prepared in 10% hydroxypropyl-β-cyclodextrin in ddH_20. ND-2158 (100 mg/kg/day) or its vehicle was administered i.p. twice per day. Ibrutinib (Pharmacyclics) was prepared in DMSO/10% hydroxypropyl-β-cyclodextrin in ddH_20 (5:95). Ibrutinib (9 mg/kg/day) or its vehicle was administered i.p. once per day. For ND-2158/ibrutinib combination experiments, ibrutinib was administered 4 h after ND-2158. ABT-199 (Selleckchem) was prepared in Phosal 50 PG/polyethylene glycol-400/ethanol (6:3:1) as previously described (Souers et al., 2013). ABT-199 (50 mg/kg/day) or its vehicle was administered once per day by oral gavage. For ND-2158/ABT-199 combination experiments, ABT-199 was administered 4 h after ND-2158. Tumor growth was monitored daily by measuring tumor size in two orthogonal dimensions by digital caliper measurement. Tumor volume was calculated by applying the following equation: tumor volume = (length × width^2)/2. The

statistical significance of tumor volume was modeled using a mixed effects model, assuming a linear relationship between time and log tumor volume, with individual mice representing random effects. P-values reported represent the significance of the time and treatment interaction term on tumor volume.

In vivo LPS-induced cytokine production model. In vivo experiments of LPS-induced TNF production were conducted at ChemPartners (Shanghai, China). Female Lewis rats (n = 10 per group) were dosed i.p. with ND-2158 (1, 3, and 30 mg/kg) or vehicle (10% hydroxypropyl-β-cyclodextrin in saline). Dexamethasone (Dex) was administered by oral gavage in 0.5% methylcellulose saline. 30 min after dosing, the rats were i.v. administered 0.1 mg/kg LPS in PBS. 1 h later, rats were bled and serum analyzed for TNF production by ELISA (eBioscience).

Collagen-induced arthritis model. Male DBA mice were immunized with type II collagen emulsified in complete Freund's adjuvant on days 0 and 21, according to the published protocol (Brand et al., 2004). Mice were randomly enrolled with disease onset (n = 8 per group, except for n = 4 naive controls). Disease onset was defined as four digits in one paw showing swelling/redness (as a symptom of arthritis; Brand et al., 2004). Day 1 indicates the first treatment day, and mice were evaluated daily for clinical scores until day 11. ND-2158 or its vehicle (10% hydroxypropyl-β-cyclodextrin in ddH_20) was administered i.p. Dex served as a positive control for blocking collagen-induced arthritis. ND-2158 was dosed at 30 mg/kg i.p. twice daily and Dex at 0.1 mg/kg i.p. twice daily. Statistics are as follows: Student's t test IRAK4 inhibitor versus vehicle: *, $P < 0.05$ days 2–11; Dex versus vehicle: *, $P < 0.05$ day 1; **, $P < 0.01$ day 2; ***, $P < 0.001$ days 3–5; ****, $P < 0.0001$ days 6–11. Histological analysis was conducted on harvested tissue sections. Histology scores are as follows: 0 = normal, 1 = minimal, 2 = mild, 3 = moderate, 4 = marked, 5 = severe.

Monosodium urate (MSU) air pouch model for gout. BALB/c mice were distributed randomly into 10 mice per group. ND-2158 or vehicle (10% hydroxypropyl-β-cyclodextrin prepared in ddH_2O) was administered i.p. (3, 10, and 30 mg/kg). After the first dose, the mice were anesthetized, and the nape of the neck was shaved to generate an air pouch by injecting 6 ml of air using a 23-gauge needle (Chen et al., 2006). Mice were subsequently dosed once daily with ND-2158 or vehicle for 6 d. 30 min after the final dose, 3 ml MSU suspension was injected into the air pouch. 4 h after the MSU injection, exudate was removed from the pouch, and an aliquot was used for WBC count and differential analysis.

Online supplemental material

Fig. S1 shows gene expression changes in four ABC DLBCL lines induced by a time course of treatment with the IRAK4 inhibitor ND-2158. Table S1, included as a separate Excel file, shows the percent inhibition in kinase activity of IRAK4 inhibitors ND-2110 or ND-2158 tested across 334 kinases. Table S2, included as a separate Excel file, lists gene signature enrichment for genes down-modulated by a time course of ND-2158 treatment in ABC DLBCL. Online supplemental material is available at http://www.jem.org/cgi/content/full/jem.20151074/DC1.

ACKNOWLEDGMENTS

We acknowledge Leah Frye, Jeremy Greenwood, Matt Wessel, Mee Shelley, Shawn Watts, and Ramy Farid (Schrödinger); Alison Bendele and Phillip Bendele (Bolder BioPath); Haiching Ma (Reaction Biology); Xinyi Huang, Lingling Liu, Lezhen Li, Ronggang Liu, and Congran Feng (Pharmaron); Feilan Wang and Yajun Xu (Chempartners); and Eric Smith (Nimbus Therapeutics) who helped prepare figures.

This research was supported by the Intramural Research Program of the National Institutes of Health (NIH), National Cancer Institute, Center for Cancer Research. We thank George Wright for statistical analysis (Biometric Research Branch, National Cancer Institute/NIH).

P.N. Kelly, Y. Yang, A.L. Shaffer III, L. Rui, and L.M. Staudt declare no competing financial interests. D.L. Romero, D. Chaudhary, W. Miao, W.F. Westlin, and R. Kapeller are employees of Nimbus Therapeutics. S. Robinson is an employee of Schrödinger. The authors declare no additional competing financial interests.

Submitted: 28 June 2015
Accepted: 9 October 2015

REFERENCES

Alizadeh, A.A., M.B. Eisen, R.E. Davis, C. Ma, I.S. Lossos, A. Rosenwald, J.C. Boldrick, H. Sabet, T. Tran, X. Yu, et al. 2000. Distinct types of diffuse large B-cell lymphoma identified by gene expression profiling. *Nature.* 403:503–511. http://dx.doi.org/10.1038/35000501

Bendele, A. 2001. Animal models of rheumatoid arthritis. *J. Musculoskelet. Neuronal Interact.* 1:377–385.

Brand, D.D., A.H. Kang, and E.F. Rosloniec. 2004. The mouse model of collagen-induced arthritis. *Methods Mol. Med.* 102:295–312.

Ceribelli, M., P.N. Kelly, A.L. Shaffer, G.W. Wright, W. Xiao, Y. Yang, L.A. Mathews Griner, R. Guha, P. Shinn, J.M. Keller, et al. 2014. Blockade of oncogenic IκB kinase activity in diffuse large B-cell lymphoma by bromodomain and extraterminal domain protein inhibitors. *Proc. Natl. Acad. Sci. USA.* 111:11365–11370. http://dx.doi.org/10.1073/pnas.1411701111

Chaudhary, D., S. Robinson, and D.L. Romero. 2015. Recent advances in the discovery of small molecule inhibitors of interleukin-1 receptor-associated kinase 4 (IRAK4) as a therapeutic target for inflammation and oncology disorders. *J. Med. Chem.* 58:96–110. http://dx.doi.org/10.1021/jm5016044

Chen, C.J., Y. Shi, A. Hearn, K. Fitzgerald, D. Golenbock, G. Reed, S. Akira, and K.L. Rock. 2006. MyD88-dependent IL-1 receptor signaling is essential for gouty inflammation stimulated by monosodium urate crystals. *J. Clin. Invest.* 116:2262–2271. http://dx.doi.org/10.1172/JCI28075

Cheng, H., T. Addona, H. Keshishian, E. Dahlstrand, C. Lu, M. Dorsch, Z. Li, A. Wang, T.D. Ocain, P. Li, et al. 2007. Regulation of IRAK-4 kinase activity via autophosphorylation within its activation loop. *Biochem. Biophys. Res. Commun.* 352:609–616. http://dx.doi.org/10.1016/j.bbrc.2006.11.068

Choe, J.Y., B. Crain, S.R. Wu, and M. Corr. 2003. Interleukin 1 receptor dependence of serum transferred arthritis can be circumvented by toll-like receptor 4 signaling. *J. Exp. Med.* 197:537–542. http://dx.doi.org/10.1084/jem.20021850

Chou, T.C. 2010. Drug combination studies and their synergy quantification using the Chou-Talalay method. *Cancer Res.* 70:440–446. http://dx.doi.org/10.1158/0008-5472.CAN-09-1947

Coffey, G., F. DeGuzman, M. Inagaki, Y. Pak, S.M. Delaney, D. Ives, A. Betz, Z.J. Jia, A. Pandey, D. Baker, et al. 2012. Specific inhibition of spleen tyrosine kinase suppresses leukocyte immune function and inflammation in animal models of rheumatoid arthritis. *J. Pharmacol. Exp. Ther.* 340:350–359. http://dx.doi.org/10.1124/jpet.111.188441

Corin, A.F., L.L. Frye, J.R. Greenwood, G.C. Harriman, C. Masse, S. Robinson, D.L. Romero, K.S. Watts, and M.D. Wessel2012 IRAK inhibitors and uses thereof. Google patent publication number WO2012097013 A1. Available at: http://www.google.com/patents/WO2012097013A1 (accessed June 10, 2015).

Davis, R.E., V.N. Ngo, G. Lenz, P. Tolar, R.M. Young, P.B. Romesser, H. Kohlhammer, L. Lamy, H. Zhao, Y. Yang, et al. 2010. Chronic active B-cell-receptor signalling in diffuse large B-cell lymphoma. *Nature.* 463:88–92. http://dx.doi.org/10.1038/nature08638

Ehlers, M., H. Fukuyama, T.L. McGaha, A. Aderem, and J.V. Ravetch. 2006. TLR9/MyD88 signaling is required for class switching to pathogenic IgG2a and 2b autoantibodies in SLE. *J. Exp. Med.* 203:553–561. http://dx.doi.org/10.1084/jem.20052438

Ferrao, R., H. Zhou, Y. Shan, Q. Liu, Q. Li, D.E. Shaw, X. Li, and H. Wu. 2014. IRAK4 dimerization and trans-autophosphorylation are induced by Myddosome assembly. *Mol. Cell.* 55:891–903. http://dx.doi.org/10.1016/j.molcel.2014.08.006

Green, N.M., and A. Marshak-Rothstein. 2011. Toll-like receptor driven B cell activation in the induction of systemic autoimmunity. *Semin. Immunol.* 23:106–112. http://dx.doi.org/10.1016/j.smim.2011.01.016

Jurk, M., G. Chikh, B. Schulte, A. Kritzler, D. Richardt-Pargmann, C. Lampron, R. Luu, A.M. Krieg, A.P. Vicari, and J. Vollmer. 2011. Immunostimulatory potential of silencing RNAs can be mediated by a non-uridine-rich toll-like receptor 7 motif. *Nucleic Acid Ther.* 21:201–214. http://dx.doi.org/10.1089/nat.2011.0298

Kawai, T., O. Adachi, T. Ogawa, K. Takeda, and S. Akira. 1999. Unresponsiveness of MyD88-deficient mice to endotoxin. *Immunity.* 11:115–122. http://dx.doi.org/10.1016/S1074-7613(00)80086-2

Kim, T.W., K. Staschke, K. Bulek, J. Yao, K. Peters, K.H. Oh, Y. Vandenburg, H. Xiao, W. Qian, T. Hamilton, et al. 2007. A critical role for IRAK4 kinase activity in Toll-like receptor-mediated innate immunity. *J. Exp. Med.* 204:1025–1036. http://dx.doi.org/10.1084/jem.20061825

Kraan, W., H.M. Horlings, M. van Keimpema, E.J. Schilder-Tol, M.E. Oud, C. Scheepstra, P.M. Kluin, M.J. Kersten, M. Spaargaren, and S.T. Pals. 2013. High prevalence of oncogenic MYD88 and CD79B mutations in diffuse large B-cell lymphomas presenting at immune-privileged sites. *Blood Cancer J.* 3:e139. http://dx.doi.org/10.1038/bcj.2013.28

Kraan, W., M. van Keimpema, H.M. Horlings, E.J. Schilder-Tol, M.E. Oud, L.A. Noorduyn, P.M. Kluin, M.J. Kersten, M. Spaargaren, and S.T. Pals. 2014. High prevalence of oncogenic MYD88 and CD79B mutations in primary testicular diffuse large B-cell lymphoma. *Leukemia.* 28:719–720. http://dx.doi.org/10.1038/leu.2013.348

Lam, L.T., R.E. Davis, J. Pierce, M. Hepperle, Y. Xu, M. Hottelet, Y. Nong, D. Wen, J. Adams, L. Dang, and L.M. Staudt. 2005. Small molecule inhibitors of IκB kinase are selectively toxic for subgroups of diffuse large B-cell lymphoma defined by gene expression profiling. *Clin. Cancer Res.* 11:28–40.

Lam, L.T., G. Wright, R.E. Davis, G. Lenz, P. Farinha, L. Dang, J.W. Chan, A. Rosenwald, R.D. Gascoyne, and L.M. Staudt. 2008. Cooperative signaling through the signal transducer and activator of transcription 3 and nuclear factor-κB pathways in subtypes of diffuse large B-cell lymphoma. *Blood.* 111:3701–3713. http://dx.doi.org/10.1182/blood-2007-09-111948

Lau, C.M., C. Broughton, A.S. Tabor, S. Akira, R.A. Flavell, M.J. Mamula, S.R. Christensen, M.J. Shlomchik, G.A. Viglianti, I.R. Rifkin, and A. Marshak-Rothstein. 2005. RNA-associated autoantigens activate B cells by combined B cell antigen receptor/Toll-like receptor 7 engagement. *J. Exp. Med.* 202:1171–1177. http://dx.doi.org/10.1084/jem.20050630

Leadbetter, E.A., I.R. Rifkin, A.M. Hohlbaum, B.C. Beaudette, M.J. Shlomchik, and A. Marshak-Rothstein. 2002. Chromatin-IgG complexes activate B cells by dual engagement of IgM and Toll-like receptors. *Nature.* 416:603–607. http://dx.doi.org/10.1038/416603a

Lenz, G., G.W. Wright, N.C. Emre, H. Kohlhammer, S.S. Dave, R.E. Davis, S. Carty, L.T. Lam, A.L. Shaffer, W. Xiao, et al. 2008. Molecular subtypes of diffuse large B-cell lymphoma arise by distinct genetic pathways. *Proc. Natl. Acad. Sci. USA.* 105:13520–13525. http://dx.doi.org/10.1073/pnas.0804295105

Li, Z.M., A. Rinaldi, A. Cavalli, A.A. Mensah, M. Ponzoni, R.D. Gascoyne, G. Bhagat, E. Zucca, and F. Bertoni. 2012. MYD88 somatic mutations in MALT lymphomas. *Br. J. Haematol.* 158:662–664. http://dx.doi.org/10.1111/j.1365-2141.2012.09176.x

Lim, J., M.D. Altman, J. Baker, J.D. Brubaker, H. Chen, Y. Chen, T. Fischmann, C. Gibeau, M.A. Kleinschek, E. Leccese, et al. 2015. Discovery of 5-Amino-*N*-(1*H*-pyrazol-4-yl)pyrazolo[1,5-*a*]pyrimidine-3-carboxamide inhibitors of IRAK4. *ACS Med. Chem. Lett.* 6:683–688. http://dx.doi.org/10.1021/acsmedchemlett.5b00107

Ma, S., A. Turetsky, L. Trinh, and R. Lu. 2006. IFN regulatory factor 4 and 8 promote Ig light chain κ locus activation in pre-B cell development. *J. Immunol.* 177:7898–7904. http://dx.doi.org/10.4049/jimmunol.177.11.7898

Marshak-Rothstein, A. 2006. Toll-like receptors in systemic autoimmune disease. *Nat. Rev. Immunol.* 6:823–835. http://dx.doi.org/10.1038/nri1957

Matera, G., A. Quirino, A. Giancotti, M.C. Pulicari, L. Rametti, M.L. Rodríguez, M.C. Liberto, and A. Focà. 2012. Procalcitonin neutralizes bacterial LPS and reduces LPS-induced cytokine release in human peripheral blood mononuclear cells. *BMC Microbiol.* 12:68. http://dx.doi.org/10.1186/1471-2180-12-68

McElroy, W.T., Z. Tan, G. Ho, S. Paliwal, G. Li, W.M. Seganish, D. Tulshian, J. Tata, T.O. Fischmann, C. Sondey, et al. 2015. Potent and selective amidopyrazole inhibitors of IRAK4 that are efficacious in a rodent model of inflammation. *ACS Med. Chem. Lett.* 6:677–682. http://dx.doi.org/10.1021/acsmedchemlett.5b00106

Ngo, V.N., R.M. Young, R. Schmitz, S. Jhavar, W. Xiao, K.H. Lim, H. Kohlhammer, W. Xu, Y. Yang, H. Zhao, et al. 2011. Oncogenically active MYD88 mutations in human lymphoma. *Nature.* 470:115–119. http://dx.doi.org/10.1038/nature09671

Pham-Ledard, A., D. Cappellen, F. Martinez, B. Vergier, M. Beylot-Barry, and J.P. Merlio. 2012. MYD88 somatic mutation is a genetic feature of primary cutaneous diffuse large B-cell lymphoma, leg type. *J. Invest. Dermatol.* 132:2118–2120. http://dx.doi.org/10.1038/jid.2012.102

Pierer, M., U. Wagner, M. Rossol, and S. Ibrahim. 2011. Toll-like receptor 4 is involved in inflammatory and joint destructive pathways in collagen-induced arthritis in DBA1J mice. *PLoS One.* 6:e23539. http://dx.doi.org/10.1371/journal.pone.0023539

Puente, X.S., M. Pinyol, V. Quesada, L. Conde, G.R. Ordóñez, N. Villamor, G. Escaramis, P. Jares, S. Beà, M. González-Díaz, et al. 2011. Whole-genome sequencing identifies recurrent mutations in chronic lymphocytic leukaemia. *Nature.* 475:101–105. http://dx.doi.org/10.1038/nature10113

Sciammas, R., A.L. Shaffer, J.H. Schatz, H. Zhao, L.M. Staudt, and H. Singh. 2006. Graded expression of interferon regulatory factor-4 coordinates isotype switching with plasma cell differentiation. *Immunity.* 25:225–236. http://dx.doi.org/10.1016/j.immuni.2006.07.009

Souers, A.J., J.D. Leverson, E.R. Boghaert, S.L. Ackler, N.D. Catron, J. Chen, B.D. Dayton, H. Ding, S.H. Enschede, W.J. Fairbrother, et al. 2013. ABT-199, a potent and selective BCL-2 inhibitor, achieves antitumor activity while sparing platelets. *Nat. Med.* 19:202–208. http://dx.doi.org/10.1038/nm.3048

Suzuki, N., S. Suzuki, G.S. Duncan, D.G. Millar, T. Wada, C. Mirtsos, H. Takada, A. Wakeham, A. Itie, S. Li, et al. 2002. Severe impairment of

interleukin-1 and Toll-like receptor signalling in mice lacking IRAK-4. *Nature.* 416:750–756. http://dx.doi.org/10.1038/nature736

Treon, S.P., L. Xu, G. Yang, Y. Zhou, X. Liu, Y. Cao, P. Sheehy, R.J. Manning, C.J. Patterson, C. Tripsas, et al. 2012. MYD88 L265P somatic mutation in Waldenström's macroglobulinemia. *N. Engl. J. Med.* 367:826–833. http://dx.doi.org/10.1056/NEJMoa1200710

Tumey, L.N., D.H. Boschelli, N. Bhagirath, J. Shim, E.A. Murphy, D. Goodwin, E.M. Bennett, M. Wang, L.L. Lin, B. Press, et al. 2014. Identification and optimization of indolo[2,3-c]quinoline inhibitors of IRAK4. *Bioorg. Med. Chem. Lett.* 24:2066–2072. http://dx.doi.org/10.1016/j.bmcl.2014.03.056

Wang, Z., J. Liu, A. Sudom, M. Ayres, S. Li, H. Wesche, J.P. Powers, and N.P. Walker. 2006. Crystal structures of IRAK-4 kinase in complex with inhibitors: a serine/threonine kinase with tyrosine as a gatekeeper. *Structure.* 14:1835–1844. http://dx.doi.org/10.1016/j.str.2006.11.001

Wang, Z., H. Wesche, T. Stevens, N. Walker, and W.C. Yeh. 2009. IRAK-4 inhibitors for inflammation. *Curr. Top. Med. Chem.* 9:724–737. http://dx.doi.org/10.2174/156802609789044407

Wilson, W.H., R.M. Young, R. Schmitz, Y. Yang, S. Pittaluga, G. Wright, C.J. Lih, P.M. Williams, A.L. Shaffer, J. Gerecitano, et al. 2015. Targeting B cell receptor signaling with ibrutinib in diffuse large B cell lymphoma. *Nat. Med.* 21:922–926. http://dx.doi.org/10.1038/nm.3884

Yang, Y., A.L. Shaffer III, N.C. Emre, M. Ceribelli, M. Zhang, G. Wright, W. Xiao, J. Powell, J. Platig, H. Kohlhammer, et al. 2012. Exploiting synthetic lethality for the therapy of ABC diffuse large B cell lymphoma. *Cancer Cell.* 21:723–737. http://dx.doi.org/10.1016/j.ccr.2012.05.024